Inflammation
https://doi.org/10.1007/s10753-024-02060-z

RESEARCH

Celastrol Regulates the Hsp90-NLRP3 Interaction to Alleviate Rheumatoid Arthritis

Junjie Yang[1] , Biyao He[1] , Longjiao Dang[1] , Jiayu Liu[1] , Guohao Liu[1] , Yuwei Zhao[1] , Pengfei Yu[1] , Qiaoyun Wang[1] , Lei Wang[1,2] and Wenyu Xin[1,2]

Received 3 April 2024; accepted 21 May 2024

Abstract—Previous studies have verified that celastrol (Cel) protects against rheumatoid arthritis (RA) by inhibiting the NLRP3 inflammasome signaling pathway, but the molecular mechanism by which Cel regulates NLRP3 has not been clarified. This study explored the specific mechanisms of Cel *in vitro* and *in vivo*. A type II collagen-induced arthritis (CIA) mouse model was used to study the antiarthritic activity of Cel; analysis of paw swelling, determination of the arthritis score, and pathological examinations were performed. The antiproliferative and antimigratory effects of Cel on TNF-α induced fibroblast-like synoviocytes (FLSs) were tested. Proinflammatory factors were evaluated using enzyme-linked immunosorbent assay (ELISA). The expression of NF-κB/NLRP3 pathway components was determined by western blotting and immunofluorescence staining *in vitro* and *in vivo*. The putative binding sites between Cel and Hsp90 were predicted through molecular docking, and the binding interactions were determined using the Octet RED96 system and coimmunoprecipitation. Cel decreased arthritis severity and reduced TNF-α-induced FLSs migration and proliferation. Additionally, Cel inhibited NF-κB/NLRP3 signaling pathway activation, reactive oxygen species (ROS) production, and proinflammatory cytokine secretion. Furthermore, Cel interacted directly with Hsp90 and blocked the interaction between Hsp90 and NLRP3 in FLSs. Our findings revealed that Cel regulates NLRP3 inflammasome signaling pathways both *in vivo* and *in vitro*. These effects are induced through FLSs inhibition of the proliferation and migration by blocking the interaction between Hsp90 and NLRP3.

KEY WORDS: celastrol; rheumatoid arthritis; fibroblast-like synoviocytes; NLRP3 inflammasome; heat shock protein 90; nuclear factor-kappa B

Junjie Yang and Biyao He contributed equally to this work.

[1]Key Laboratory of Prescription Effect and Clinical Evaluation of State Administration of Traditional Chinese Medicine of China, School of Pharmacy, Binzhou Medical University, Yantai 264003, China

[2]To whom correspondence should be addressed at Key Laboratory of Prescription Effect and Clinical Evaluation of State Administration of Traditional Chinese Medicine of China, School of Pharmacy, Binzhou Medical University, Yantai, 264003, China. Email: wanglei424@163.com xinwenyu1391139@163.com

Abbreviations CFA, Complete Freund's adjuvant; DAPI, 4′,6-Diamidino-2-phenylindole; DCFH-DA, Dichlorofluorescein Diacetate; Dex, Dexamethasone; EDTA, Ethylene Diamine Tetraacetic Acid; EDU, 5-Ethynyl-2'-deoxyuridine; ELISA, Enzyme-linked immunosorbent assay; FLSs, Fibroblast-like synoviocytes; Hsp90, Heat shock protein 90; IFA, Incomplete Freund's adjuvant; IL-10, Interleukin-10; IL-1β, Interleukin-1β; MTX, Methotrexate; NF-κB, Nuclear factor-kappa B; NLRP3, NOD-like receptor thermal protein domain associated protein 3; ROS, Reactive oxygen species; SGT1, The suppressor of the G2 allele of skp1; TGF-1β, Transforming growth factor-β; TNF-α, Tumor necrosis factor-α

Published online: 14 June 2024

INTRODUCTION

Rheumatoid arthritis (RA) is a chronic autoimmune disease with a global incidence of 1%. RA is mainly characterized by synovial hyperplasia, inflammatory cell infiltration, bone and cartilage degradation and damage [1, 2]. The abnormal proliferation of synovial cells is one of the main pathological features of RA [3, 4]. The physiological role of fibroblast-like synoviocytes (FLSs) in RA is mainly attributed to FLS-mediated damage to articular bone and cartilage supporting structures [5, 6].

Celastrol (Cel) is extracted from the root bark of *Tripterygium wilfordii* and is the main active compound, producing various pharmacological effects. Studies have shown that Cel can be used for the treatment of RA [7]. The abnormal activation of NLRP3 inflammasome has been associated with a variety of human inflammatory diseases [8]. Previous research has shown that Cel inhibits inflammatory responses and signal transduction in the NLRP3 inflammasome [9]. However, whether Cel can restrain FLSs proliferation and migration by regulating the NLRP3 inflammasome has not been studied or elucidated. In this study, the effect of Cel on the proliferation and migration of TNF-α-stimulated FLSs were investigated, and the molecular mechanism involved in the signaling pathway of the NLRP3 inflammasome was further investigated.

Moreover, studies have shown that Cel, a heat shock protein 90 (Hsp90) inhibitor, exerts an antitumor effect through Hsp90 [10, 11]. HSP90 is a known intracellular chaperone that regulates inflammatory processes, including the secretion of NLRP3 inflammasome and pro-inflammatory cytokine interleukin (IL)-1b [12]. It is also a central regulator of important processes, including stress regulation, regulation of protein substrate (client) stability, immune responses, protein folding, and many other processes [13–15]. Hsp90 has been established as a molecular chaperone involved in the inflammatory response of RA, but its role in synovial hyperplasia and bone destruction remains uncertain. Moreover, Hsp90 inhibitors can effectively modulate inflammation through TGF-1β and IL-10 and show activity in RA [16, 17]. Importantly, Hsp90 also plays a critical role in maintaining the stability of the NLRP3 inflammasome.

Previous studies have shown that NLRP3 may be a client protein of Hsp90 [18]. Without Hsp90, NLRP3 may misfold before degradation by the proteasome [19]. Studies have shown that Hsp90 and NLRP3 interact with the ubiquitin ligase-associated protein SGT1 and that the stability of NALP3 is affected by continuous inhibition of Hsp90. The Hsp90-SGT1 complex keeps NLRP3 inactive but has the ability to activate this molecule [20]. In addition, Hsp90 is necessary for inflammation and to protect NLRP3 from autophagic degradation and the proteasome [12, 21]. Moreover, Hsp90 inhibitors can inhibit the activity of the inflammasome, block the activation of the Nod2-mediated transcription factor NF-κB, and decrease NALP3-mediated gout-like inflammation [18]. Our previous research showed that Cel inhibits reactive oxygen species (ROS) production and the NF-κB signaling pathway (the first signal) via the second signal of NLRP3, thereby inhibiting the activation and assembly of the NLRP3 inflammasome. However, whether Cel protects against RA by regulating the NLRP3 inflammasome signaling pathway and Hsp90 has not been elucidated.

Our previous studies have found that Cel has a very good therapeutic effect on RA, and its therapeutic effect exerts anti-inflammatory effects by inhibiting NLRP3 inflammasome [9]. As a new target for the treatment of RA, the binding of NLRP3 client protein Hsp90 to Cel and the binding mode are still unknown. In this study, in order to reveal the binding mode of Cel and Hsp90, and how it affects the expression of NLRP3 inflammasome, so as to play a role in the treatment of RA. We first studied the effect of Cel on NF-κB/NLRP3 signaling pathway in collagen-induced arthritis (CIA) mouse model through *in vivo* experiments. After that, we explore the specific mechanism of Cel in the treatment of RA based on Hsp90/NLRP3 signaling pathway. Last but not the least, WB and Co-IP were used to study the effect of Cel on Hsp90-NLRP3 complex and Hsp90/NLRP3 signaling pathway in TNF-α-induced FLS cell model.

MATERIALS AND METHODS

Reagents and Antibodies

Cel (Fig. 1a; purity ≥ 98%), methotrexate (MTX; purity ≥ 99%) and enzyme-linked immunosorbent assay (ELISA) kits for IL-1β, IL-6, and TNF-α were acquired from Solarbio (Beijing, China). Dexamethasone (Dex; purity = 97%), tumor necrosis factor-α (TNF-α) and MTT were obtained from Sigma–Aldrich (Saint Louis, MO, USA). Chick type II collagen (CII), complete Freund's adjuvant (CFA, 1 mg/mL), and incomplete Freund's adjuvant (IFA, 1 mg/mL) were acquired from

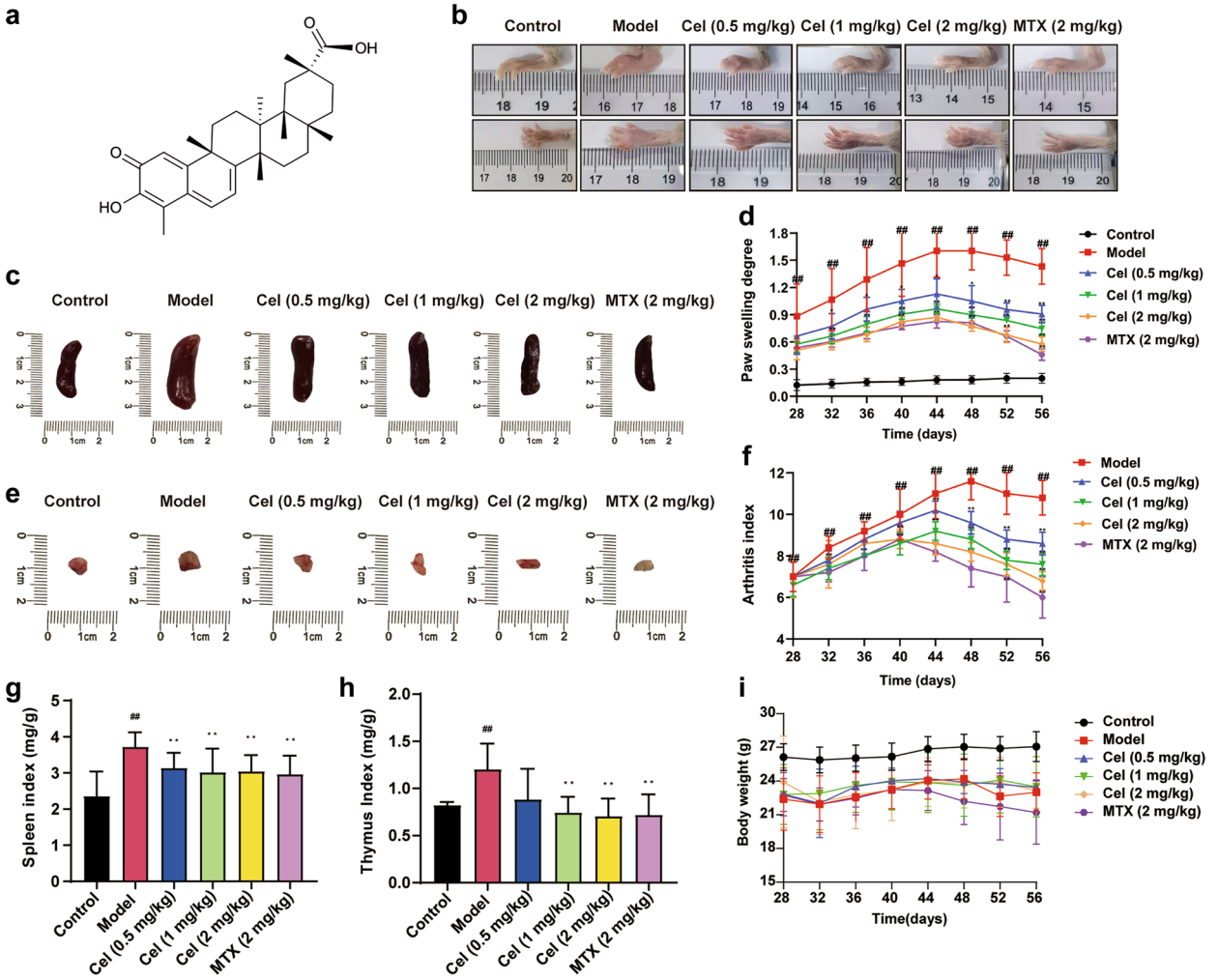

Fig. 1 Cel disrupts CIA progression and improves metabolism and immunity. (**a**) Chemical structure of Cel. (**b**) Images of the joints of the mice. (**c**) Images of the mice spleen. (**d**) Paw swelling degree were measured via plethysmometer. (**e**) Images of the mice thymus. (**f**) Cel treatment reduced the arthritis index score of CIA mice. (**g**, **h**) Cel treatment improved the spleen index (**g**) and thymus index (**h**) of CIA mice. (**i**) Body weight of treated mice over time. Data were presented as mean ± SD (n = 6). $^{\#\#}P < 0.01$ vs. control; $^{*}P < 0.05$, $^{**}P < 0.01$ vs. model group.

Chondrex, Inc. (Redmond, WA, USA). The Active Oxygen Detection Kit was purchased from Beyotime Biotechnology Co., Ltd. (Shanghai, China). An EdU cell proliferation assay kit was obtained from Ribo Biotechnology Co., Ltd. (Guangzhou, China), and a coimmunoprecipitation (Co-IP) kit was obtained from Absin Biotechnology Co., Ltd. (Shanghai, China). Primary antibodies against pp65, p65, p-IκB-α, NLRP3, Hsp90, ASC, vimentin, normal rabbit IgG, and GAPDH were obtained from Cell Signaling Technology (Beverly, MA, USA). An anti-cleaved caspase-1 antibody was purchased from R&D Systems (MN, USA). The anti-Hsp90 antibody was purchased from Abcam (Cambridge, UK), and the anti-CD68 antibody was purchased from Novus Biologicals (CO, USA).

Animals

Seven-week-old male DBA/1 (SPF, 18 ± 22 g) mice were procured from Changzhou Cavens Laboratory Animal Co., Ltd. [SCXK(SU)2016-0010, Jiangsu, China] and fed at the Laboratory Animal Centre of Binzhou Medical

University. Except for during the fasting test, the animals had free access to food and water throughout the trial period. All mice were fed according to the experimental standards authorized by the Animal Ethics Committee of Binzhou Medical University.

CIA Model Induction

The CIA model was established in 8-week-old mice according to the previously described methods [22]. An equal volume of CII (2 mg/mL, Chondrex, Inc., Redmond, WA, USA) and CFA (Chondrex, Inc.) were fully mixed in an EP tube and sonicated on ice until complete emulsification. On day 0, 100 μL emulsion was injected subcutaneously into the tail root (1–2 cm) of mice. On day 21, the equal volume of CII was added to IFA (Chondrex, Inc.), and the emulsion was prepared by the same method, and 100 μL of enhanced immunity was injected into the tail root of mice.

Drug Administration

The CIA model mice were randomized into five experimental groups of 6 mice each: model, MTX (2 mg/kg), and Cel (0.5 mg/kg, 1 mg/kg and 2 mg/kg) groups. Unmodeled mice composed the control group (n = 6). After the second immunization, Cel and MTX were administered to the mice with CIA by gavage once a day. Furthermore, the control group and the model group were administered 0.5% sodium carboxymethyl cellulose (CMC-Na) by gavage once a day. The dose of Cel used in this research was based on previous studies and preliminary experiments [9]. On day 56, the mice were removed, and the serum was collected and stored for subsequent analysis.

Body Weight and Paw Swelling Measurements

A toe measuring instrument (PV-200, Chengdu Tai Meng Technology Co., Ltd., Chengdu, China) was used to measure paw swelling, and the body weights of the mice were measured using an electronic scale. Briefly, from day 28 to day 56, the left paw volume of each mouse was measured every 4 days as an indicator of paw swelling, and the body weights of the mice with CIA were measured.

Arthritis Score

The degree of inflammation in the mice with arthritis was observed daily. The clinical arthritis score was used to assess the development of the disease based on previously established identification criteria [23]. The total score of each mouse was used as the arthritis index, and the maximum value was 12 (3 points × 4).

Visceral Index

At 56 days after immunization, the thymus and spleen were completely removed, and the organ indices were calculated. The organ indices are reported as the weight of each immune organ relative to the body weight of the mice (mg/g).

Histological Examination

For standard histological assessments, when the mice were euthanized on day 56, the ankle joints, liver, and kidney were isolated and fixed with a 4% paraformaldehyde solution for 72 h, after which the ankle joints of the mice with CIA were decalcified with EDTA. After the joints softened, they were subjected to gradient dehydration, embedded in paraffin, and cut into thin slices. Hematoxylin and eosin (H&E) staining was performed to observe pathological changes in the tissues under an optical microscope. The samples were evaluated and scored according to previously reported methods.

Radiography

After sampling, 3 mice were randomly chosen, and the left posterior bone and joints of the mice with CIA were removed for molybdenum target radiography. X-ray imaging was performed on the breast molybdenum target instrument of the affiliated hospital, and the parameters were set to 30 kVp and 90 mA.

Microcomputed Tomography (micro-CT) Analysis

Three mice with CIA were randomly selected from each group for micro-CT (PerkinElmer, Waltham, MA, USA) detection of the left posterior joint. The specific criteria for the micro-CT ankle bone destruction score were as follows: 0) normal, 1) slight bone destruction, 2) moderate bone destruction, 3) severe bone destruction, and 4) ankylosis [24].

Cell Culture and Activity

FLSs were obtained from Yantai University (Yantai, China). The specific extraction method can be seen in the above studies [25]. The experimental samples were from

three batches of different tissues, and each experiment was repeated three times. The 4-8 generations of FLSs were selected for use in subsequent experimental research [26].

After seeding on plates, the FLSs were divided into the control group, model group, Cel groups (12.5, 25, and 50 nM) and Dex (50 nM) group, and incubated with different drugs for 2 h. After which TNF-α (10 ng/mL) was added to each well. The impact of Cel on the proliferation of FLSs was determined using the MTT assay.

In addition, the TNF-α-induced proliferation of FLSs was detected by an EdU assay. After 48 h of incubation with EdU (10 μM), the cells were infiltrated with 4% paraformaldehyde and disrupted with 0.5% Triton X-100. Then, Hoechst 33342 reaction solution was added to stain the nucleus. The FLSs were immediately photographed with a high content screening system (PerkinElmer, Llantrisant).

FLSs were cultured in 96-well plates, treated with Cel or Dex for 2 h, and induced with TNF-α for different durations until the appropriate measurements were recorded to analyze the anti-inflammatory effects of Cel.

Scratch Wound Healing Experiment

FLSs were inoculated in 6-well plates at a density of 5×10^4 cells per well. Then, the cells were cultured in an incubator for 24 h, and the monolayer surface was scratched with tips of sterile 200 μL microneedles. The cell fragments were removed with PBS, and then, fresh DMEM/F12 was added. Before TNF-α stimulation, cells in the appropriate wells were pretreated with Dex or Cel for 2 h. The 6-well plates were removed at 0 and 48 h after injury, and the scratch wounds were imaged with an inverted phase-contrast microscope (Olympus, Tokyo, Japan).

Cytokine Determination

For *in vitro* studies, the supernatant of FLSs was collected and centrifuged after 48 h of stimulation with TNF-α and stored at -80 °C. The inflammatory cytokine levels in mouse serum and cell supernatants were detected in strict accordance with the instructions of the ELISA kit.

Intracellular ROS Detection

The level of ROS in FLSs was determined using the DCFH-DA method. Briefly, after drug treatment, the cells were incubated with DCFH-DA for 30 min. Then, the intracellular ROS level was detected with a high content screening system.

Immunofluorescence Staining

The ankle joint tissues were dewaxed, dehydrated, sealed, incubated, rinsed with PBS, and sliced for antigen repair. Goat serum was added to the FLSs, and the cells were incubated at room temperature for 30 min for blocking. After the blocking solution was added, diluted primary antibody against NLRP3 was added to the sections, which were incubated at 4 °C overnight. On the second day, the sections were rinsed with PBS, and fluorescently labeled secondary antibodies were added. The sections were incubated at 37 °C for 30 min and washed with PBS. The sections were stained with DAPI and incubated at room temperature. After the slides were rinsed with sterile PBS, they were sealed with antifluorescent quenchers and photographed using a high content screening system.

FLSs were subjected to immunofluorescence staining to determine their purity, and the expression of cleaved caspase-1 and NLRP3 and the nuclear translocation of p65 were determined. After different treatments, 50 μL of 4% paraformaldehyde was added to the FLSs in each well, and the cells were fixed at room temperature for 30 min. Then, 50 μL of 0.3% Triton X-100 was added to each well, and the cells were incubated for 15 min for cell membrane penetration. Subsequently, the FLSs were blocked with 1% sterile BSA for 30 min. Primary antibodies against vimentin, CD68, p65, NLRP3 and cleaved caspase-1 (1:200) were incubated with the FLSs overnight at 4 °C. Finally, the fluorescent dye-conjugated secondary antibody working solution was added, and the cells were incubated at room temperature in the dark for 2 h. After the FLSs nuclei were stained with DAPI, a high content screening system was used to immediately obtain images.

Western Blotting

Total protein was extracted from FLSs or joint tissues with RIPA buffer. The protein concentration was determined according to the instructions of the BCA kit. According to the prepared separation gel and concentrating gel, 30 μg of protein sample was added to each well of the gel for electrophoresis. Moreover, the proteins were transferred to a PVDF membrane. The PVDF membrane was placed in a closed solution and incubated at room temperature for 2 h. The specific primary antibodies against p65, p-p65, p-IκBα, cleaved caspase-1, ASC, NLRP3 and GAPDH (1:1000 dilution for all) were incubated with the membrane at 4 °C overnight. Then, the membranes was placed in the corresponding diluted

secondary antibody working solution and incubated at room temperature for 2 h. Finally, the luminescent liquid was added to the enhanced chemiluminescence (ECL) immunoblotting imaging system (ChemiDoc TM XRS; Bio-Rad Shanghai, China), followed by exposure and imaging, and the gray values were assessed to calculate the relative expression.

Molecular Docking

The molecular docking program was used according to the C-DOCKER protocol of Discovery Studio 2017 R2. Briefly, the human Hsp90 N-terminal crystal structure (PDB code: 2CCS) was acquired from the Protein Data Bank database. For the preparation of ligands, Discovery Studio 2017 R2 was used to generate and minimize the 3D structures of Cel and geldanamycin. Protein preparation requires the addition of hydrogen atoms, the removal of water molecules, and the use of the CHARMM force field. Binding sites were identified using the Find Sites From Receptor Cavities tool under Receptor–Ligand Interactions. The compounds were subjected to molecular docking. After molecular docking, the type of interaction between the docking protein and the ligand was analyzed.

Co-IP

FLSs were treated with or without Cel (50 nM) and placed in precooled lysis buffer. An anti-Hsp90 antibody (EPR16621-67, 1:200, Abcam Biomedicine, UK) and Protein A/G agarose were added to the lysate and incubated at 4 °C overnight. After the immunoprecipitation reaction, the cells were centrifuged (10,000 × g) for 10 min in a precooled centrifuge. After being fully washed with lysis buffer, the immunoprecipitate was boiled in loading buffer, and the proteins were detected using western blotting.

Affinity Determination

The interaction between Cel and Hsp90 was detected using a super streptavidin (SSA) biosensor in the Octet RED96 system (ForteBio, Inc., Menlo Park, CA, USA). First, the extracellular domain of the recombinant human Hsp90 protein (Abiocenter Biotechnology Co., Beijing) was biotinylated in PBS (0.1% BSA and 0.05% Tween-20) and loaded onto the SSA biosensor at 119 μg/mL. The biosensors were blocked with biocytin (5 μg/mL) for 60 s. Cel diluted in PBS (0.1% BSA, 0.05% Tween-20 and 10% DMSO) was added to the SSA biosensor loaded with Hsp90. By subtracting the nonspecific binding of Cel to the SSA biosensor, the real-time binding response (Δλ is nanometer, nm) between Cel and Hsp90 was calculated. Octet 8.5 data analysis software (ForteBio, Inc., Menlo Park, CA, USA) was used to perform nonlinear global fitting of the data, and the kinetic parameters and affinities were obtained.

Statistical Analyses

All the data were analyzed using SPSS 20.0 software and are presented as the mean ± standard deviations (mean ± SD). The data were statistically significant according to ANOVA and were normally distributed, which satisfied the assumption of homogeneity of variance. The Dunnett test was used to evaluate the significance of pairwise comparisons. $P < 0.05$ was considered to indicate statistical significance.

RESULTS

The Impact of Cel on paw Swelling and Arthritis Scores in Mice with CIA

The mice with CIA exhibited arthritis characterized by multijoint inflammation, such as swelling, erythema, joint rigidity and deformity (Fig. 1b). Compared to the model mice, the mice treated with Cel (1 mg/kg), Cel (2 mg/kg) and MTX (2 mg/kg) exhibited a reduced degree of paw swelling from day 28 to day 56 (Fig. 1d). The Cel and MTX (2 mg/kg) groups exhibited significant reductions in the arthritic index from day 28 to day 56 (Fig. 1f). Compared with the model group, the immune organ indices of the Cel- and MTX-treated groups were significantly lower (Fig. 1c, e, g, h). However, Cel had no effect on the body weight of the mice, indicating that Cel was nontoxic to the mice during the experiment (Fig. 1i).

Effect of Cel on Histopathological Changes in the Liver, Kidney and Ankle Joints of the Mice with CIA

In the control group, the joint structure of the mice was normal, and the joint surface was smooth. Synovial hyperplasia and substantial inflammatory cell infiltration were observed in the model group (Fig. 2a). Cel and

MTX (2 mg/kg) reduced inflammation, synovial cell proliferation, bone destruction, and histopathological scores in the treated animals (Fig. 2a, f).

Moreover, no marked changes in the morphology of hepatic lobules or hepatocytes or in the infiltration of inflammatory cells in the central vein were observed in the Cel (2 mg/kg) group (Fig. 2c). Additionally, no proliferation of renal tubules, no obvious morphological changes in renal tubular epithelial cells and no inflammatory cell infiltration around the glomeruli were observed (Fig. 2d). The results indicated that Cel did no induce obvious hepatorenal toxicity in mice within 56 days.

Cel Inhibits Bone Destruction in the Ankle Joints of the Mice with CIA

Radiographic imaging indicated that the joints of the mice with CIA exhibited diffuse soft tissue swelling, joint space narrowing, bone and cartilage erosion and damage (Fig. 2b). After treatment with Cel and MTX, bone damage and erosion were markedly improved, and the degree of joint space stenosis was relatively reduced (Fig. 2b). Furthermore, micro-CT was used to analyze bone destruction in the ankle joints of the mice. A clear joint structure and smooth joint surface were observed

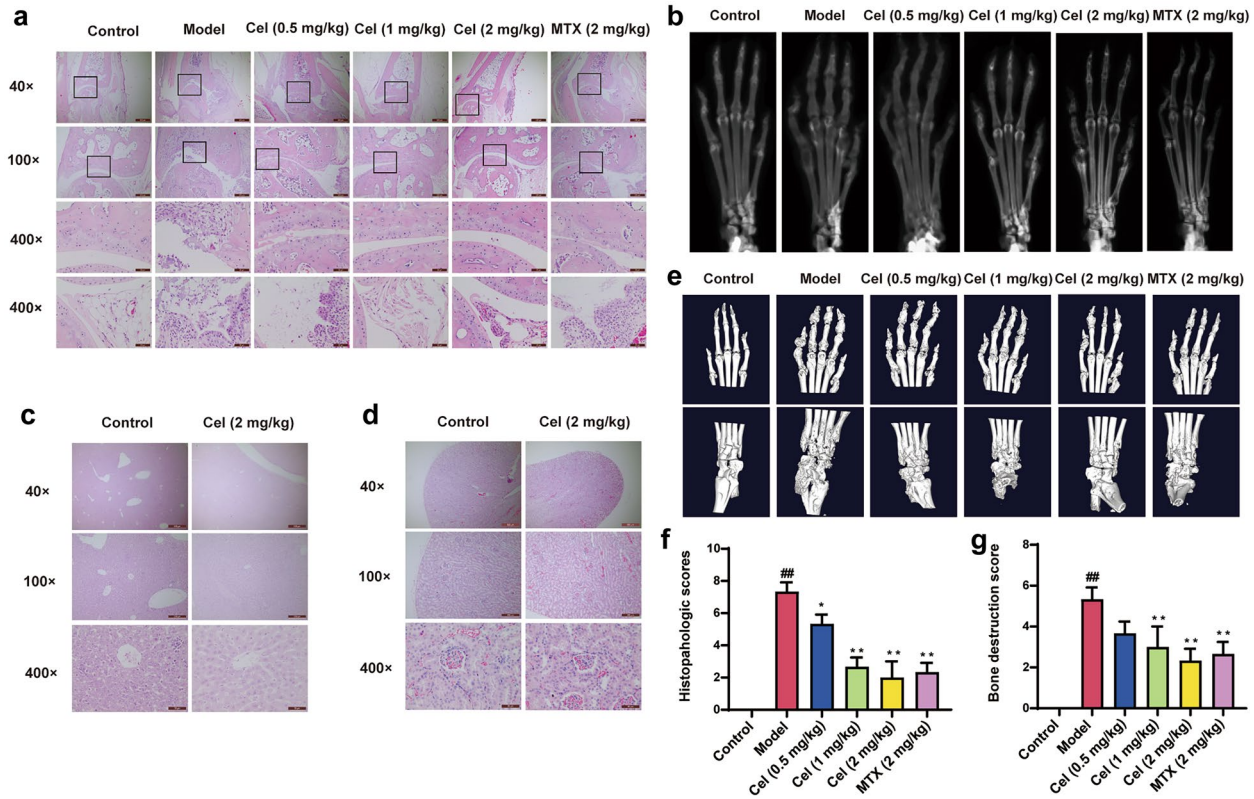

Fig. 2 Delayed treatment with Cel reduces ankle joint damage in CIA mice. (**a**) Damage to joint tissues was assessed via HE staining, with representative images shown for all treatment groups. Original magnification, 40×; high-power views, 100×and 400×. (**b**) Results of the soft tissue X ray examination of the joint of CIA mice. (**c**, **d**) Damage to liver (**c**) and kidney (**d**) tissues was assessed via HE staining, with representative images being shown for the high-dose treatment groups. Original magnification, 40×; high-power views, 100×and 400×. (**e**) Results of the micro-CT analysis. (**f**)The histopathological score was assigned to ankle joints. (**g**) The bone destruction score was assigned to the ankle joints using micro-CT determination. Data were presented as mean ± SD (n = 6). $^{\#\#}P < 0.01$ vs. control; $^{*}P < 0.05$, $^{**}P < 0.01$ vs. model group.

in the control group mice (Fig. 2e). In the model group, the bone surface of the ankle joint was rough, joint erosion was severe, the joint surface was fused, and the bone destruction score was significantly increased (Fig. 2e, g). Importantly, similar to MTX, Cel significantly alleviated ankle joint destruction and decreased the bone destruction score (Fig. 2g).

The Impact of Cel on the NLRP3 Inflammasome Signaling Pathway in Mice with CIA

We mesured the serum levels of IL-1β and TNF-α to evaluate the effects of Cel on the inflammatory response in mice with CIA. The results indicated that the expression levels of IL-1β and TNF-α in the model mice were significantly increased, and Cel (1 mg/kg or 2 mg/kg) and MTX (2 mg/kg) treatment significantly reduced TNF-α and IL-1β secretion (Fig. 3a, b). Moreover, the expression of NLRP3, ASC, cleaved caspase-1, p-p65 and p-IκBα in the ankle tissue of the mice with CIA was significantly increased (Fig. 3c–l). In contrast, Cel and MTX markedly decreased the expression of NLRP3, ASC, cleaved caspase-1, p-p65 and p-IκBα (Fig. 3c-l). These findings suggest that the protective effect of Cel on joint injury in mice with CIA is at least partially achieved by inhibiting the NLRP3 inflammasome pathway.

Effect of Cel on TNF-α-Induced FLSs Proliferation and Migration

The results of FLSs identification showed that FLSs adhered to the wall and grew in a long spindle or spindle shape (Fig. 4a). FLSs were positive for vimentin and negative for CD68 (Fig. 4b, c), indicating that the purity of FLSs was greater than 90%. Moreover, that administration of Cel concentrations less than 62.5 nM had no toxic effects on FLSs and did not affect cell growth within 48 h (Fig. 4e).

FLSs proliferation and migration are crucial mediators of RA pathology. TNF-α treatment significantly promoted (Fig. 4d), while Cel and Dex significantly reduced TNF-α-induced FLSs proliferation (Fig. 4d, f, h). We performed a scratch wound healing experiment to determine the impact of Cel on FLSs migration and found that TNF-α treatment significantly increased FLSs migration (Fig. 4g, i). Compared with TNF-α-treated cells, Cel- and Dex-treated cells exhibited significantly decreased cell migration (Fig. 4g, i).

The Impact of Cel on the NLRP3 Inflammasome Pathway in FLSs

ELISA results indicated that the levels of IL-1β and IL-6 in the supernatant of the TNF-α group were significantly increased (Fig. 5a, b). However, after pretreatment with different doses of Cel and Dex, the levels of the corresponding inflammatory factors in the supernatant of FLSs were significantly reduced (Fig. 5a, b). Western blotting and immunofluorescence staining were used to determine the impact of Cel on the NLRP3 pathway in FLSs. The expression of NLRP3, ASC, cleaved caspase-1, p-p65 and p-IκBα and the production of ROS (Fig. 5c–r) were increased after TNF-α treatment. Cel (25 or 50 nM) and Dex decreased the upregulation of these proteins and decreased the ROS level, thus inhibiting the NLRP3 inflammasome pathway (Fig. 5c–r).

The Impact of Cel on the Binding of Hsp90 to NLRP3

The results of molecular docking indicated that the main forces involved were hydrogen bonding and van der Waals forces. The hydroxyl group of Cel forms a strong hydrogen bond with ThrA:184, and the hydroxyl group on the carboxyl group forms a salt bridge with lysine A:58 (Fig. 6a). The molecular docking results of geldanamycin (GDM) with Hsp90 showed that the same amino acid, lysine A:58, of Hsp90 had strong hydrogen bonding with geldanamycin (Fig. 6b). The remaining amino acids interact through van der Waals forces around the molecule. The docking energies of Cel and geldanamycin to the Hsp90 protein were 41.3443 kJ·mol-1 and 53.3522 kJ·mol-1, respectively (Fig. 6a, b).

The binding affinity of Cel or geldanamycin to Hsp90 was determined with the Octet RED96 system. Real-time analysis revealed a specific interaction between Cel and Hsp90 [Kd = 1.04 mM, coefficient of determination (r^2) = 0.977] (Fig. 6c). Geldanamycin was used as the positive control with a Kd = 14.9 μM [coefficient of determination (r^2) = 0.9779] (Fig. 6d). Coimmunoprecipitation revealed that Hsp90 binds to NLRP3 in FLSs, and Cel pretreatment decreased the level of NLRP3 in the precipitate (Fig. 6e). These findings suggested that Cel can inhibit the binding of Hsp90 to NLRP3 by binding to Hsp90.

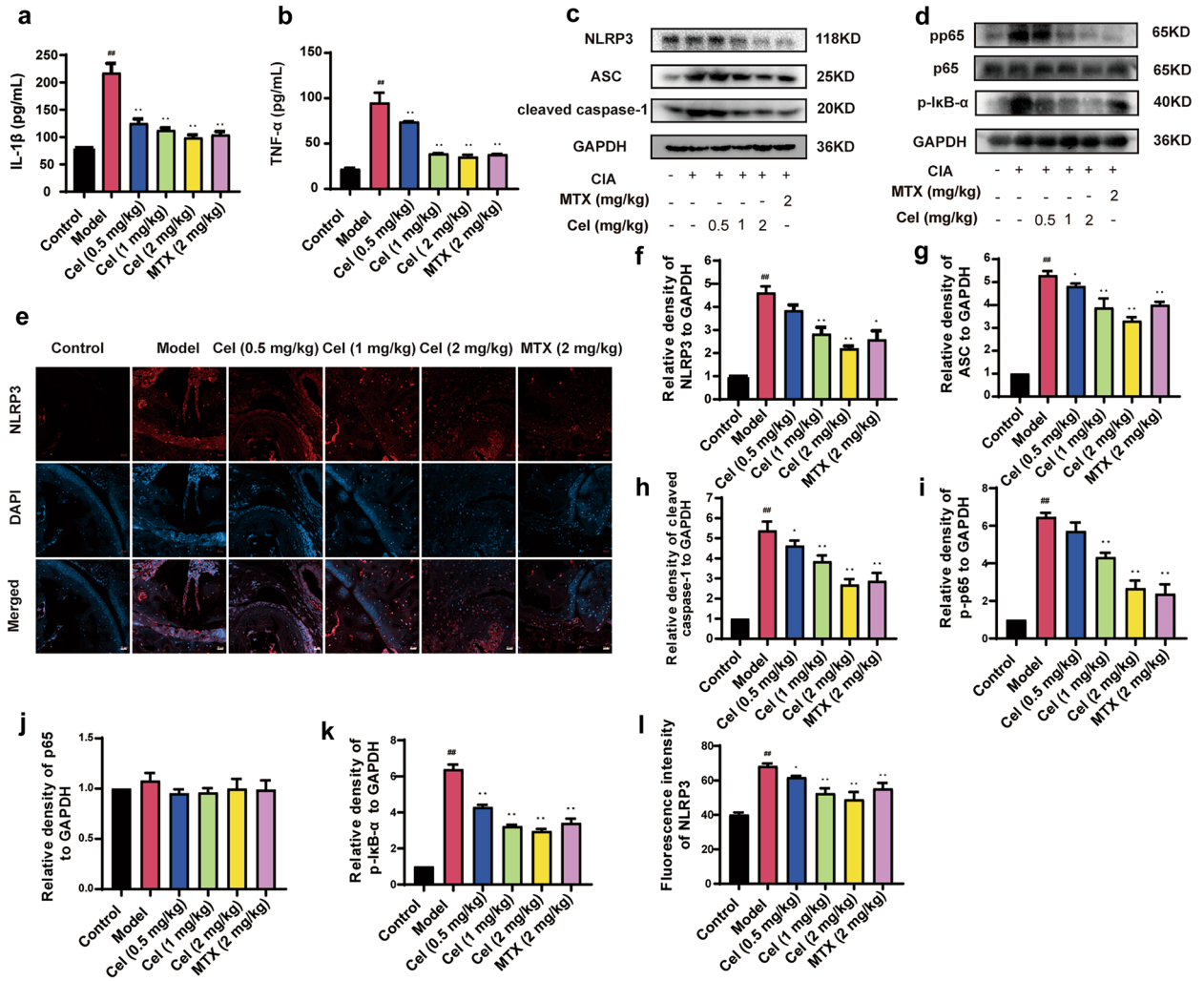

Fig. 3 Cel alters NLRP3 inflammasome pathway activation in ankle joint tissue (**a**, **b**) The serum levels of TNF-α (**a**) and IL-1β (**b**) in mice were measured via ELISA. (**c**, **f**–**h**) Western blotting was used to measure NLRP3, ASC and cleaved caspase-1 levels in joint tissue. (**d**, **i**–**k**) The expression of p-p65, p65 and p-IkB-α in the joint tissue of CIA mice was measured via western blotting. GAPDH served as a normalization control. (**e**, **l**) Immunofluorescence staining was performed to measure NLRP3 expression in joint tissue (scale bar = 20 μm). Data were presented as mean ± SD (n = 6). $^{\#\#}P < 0.01$ vs. control; $^{*}P < 0.05$, $^{**}P < 0.01$ vs. model group.

DISCUSSION

Our study revealed that Cel significantly reduced the levels of RA-related indicators, inhibited pathophysiological changes in inflammatory joints, and had no toxic effects on the liver or kidney in mice during the administration cycle. More importantly, Cel decreased the release of proinflammatory cytokines in the mice with CIA and TNF-α-induced FLSs and inhibited FLSs proliferation and migration. The above results further prove that Cel can exert an anti-RA effect by restraining the release of inflammatory factors and the abnormal proliferation and migration of FLSs, reducing joint and cartilage damage and bone erosion.

The NLRP3 inflammasome signaling pathway is closely related to the release of proinflammatory factors. Numerous studies have reported that NLRP3 inflammasome-related gene polymorphisms are associated with the severity, susceptibility, and effects of therapy on autoimmune diseases, such as RA [27–29]. Treatment

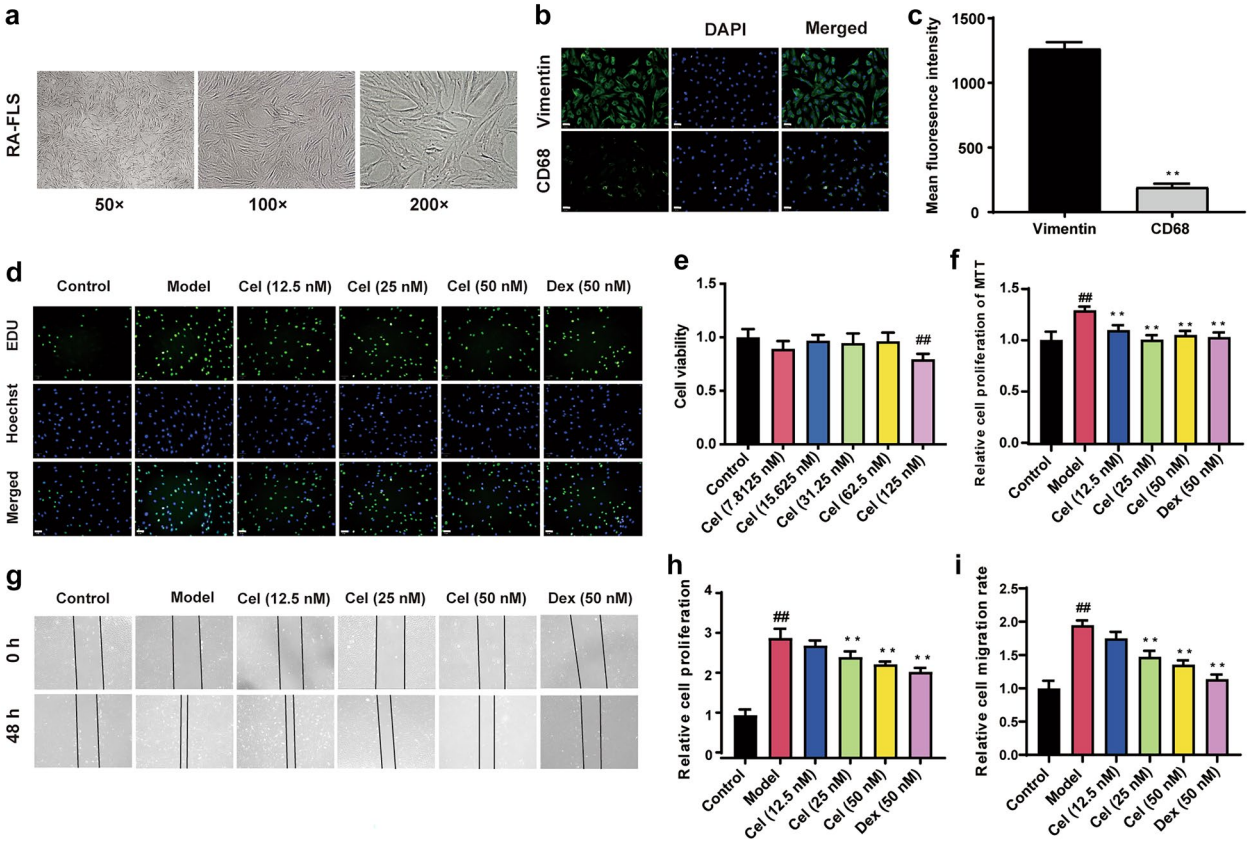

Fig. 4 Cel inhibits the proliferation and migration of FLSs. (**a**) FLSs morphology was assessed by light microscopy (50×, 100×, and 200×). (**b**, **c**) Cells were stained for vimentin or CD68 (green) and with DAPI (blue), with FLSs being vimentin-positive and CD68-negative (scale bar = 50 μm). (**d**, **h**) FLSs proliferation was also assessed based on EdU (green) incorporation, with Hoechst-stained nuclei shown in blue (scale bar = 50 μm). (**e**) Cell viability was assessed via MTT assay after a 48 h treatment with the indicated concentrations of Cel. (**f**) Following the Cel or Dex pretreatment, FLSs were treated with 10 ng/mL TNF-α for 48 h, after which an MTT assay was conducted to quantify cell proliferation. (**g**, **i**) Cell migration in a scratch wound healing assay was quantified following a 48h incubation with or without the indicated Cel and Dex (100× magnification). Data were presented as the mean ± SD from three independent experiments. $^{\#\#}P < 0.01$ vs. control; $^{*}P < 0.05$, $^{**}P < 0.01$ vs. TNF-α group or vimentin group.

with MCC950-selective NLRP3 inhibitors can alleviate arthritis symptoms and cartilage destruction, revealing that drugs targeting the NLRP3 inflammasome may be a potential therapeutic strategy for treating RA [28, 30]. Similarly, our results indicated that Cel reduced the expression of related proteins in the joints of mice with CIA and FLSs. The above results show that Cel can promote the degradation of the NLRP3 inflammasome. This means that NLRP3 is an effective potential target for Cel in the treatment of RA, and also means that Cel has a good anti-inflammatory effect.

NF-κB and ROS play important roles in the NLRP3 inflammasome signaling pathway. The activation of primary and secondary signals in the NLRP3 inflammasome signaling pathway is mainly caused by the activation of NF-κB and the production of ROS, which promote the release of proinflammatory factors and the assembly, activation and maturation of the NLRP3 inflammasome [31–33]. Therefore, inhibiting NF-κB activation and ROS production is the key to inhibiting the NLRP3 inflammasome signaling pathway. Cel decreased the nuclear translocation of p65 and ROS production in TNF-α-induced FLSs both *in vitro* and *in vivo* and reduced the expression of p-p65 and p-IκB-α. The above results indicate that Cel can inhibit the synthesis and activation of NLRP3 inflammasome by inhibiting its upstream signaling pathway, and then inhibit the secretion of downstream inflammatory factors. The above results indicate that the main anti-inflammatory

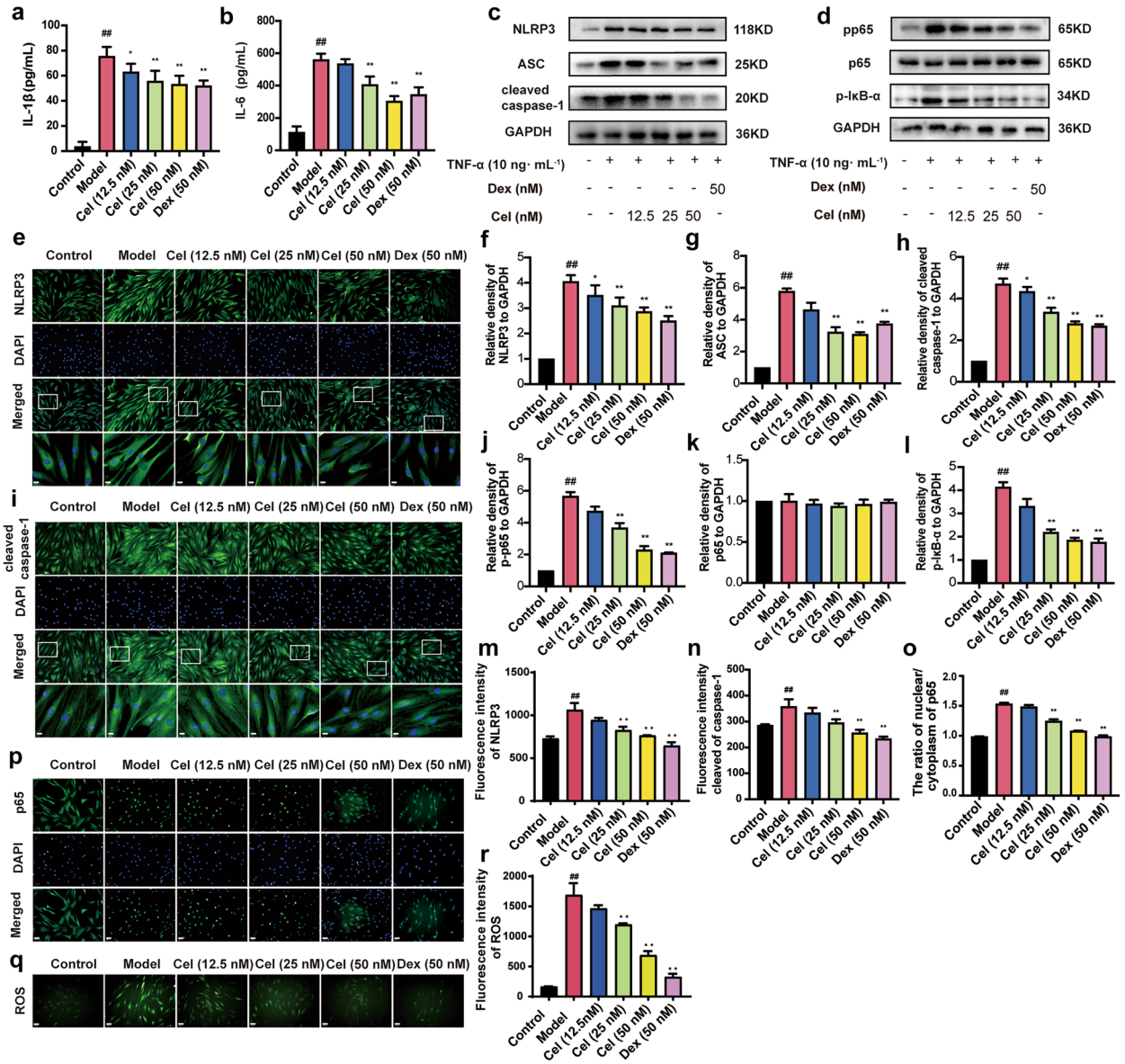

Fig. 5 Cel alters TNF-α-induced NLRP3 inflammasome pathway activation in FLSs. (**a**, **b**) Production of the proinflammatory cytokines IL-1β (**a**) and IL-6 (**b**) in TNF-α-induced FLSs supernatants was measured via ELISA. (**c**, **f**–**h**) NLRP3, ASC and cleaved caspase-1 levels were assessed in TNF-α-induced FLSs via western blotting. (**d**, **j**-**l**) p-p65, p65, and p-IkB-α levels in FLSs were measured via western blotting. GAPDH served as a normalization control. (**e**, **m**) NLRP3 levels in FLSs were assessed via immunofluorescence staining. (**i**, **n**) Cleaved caspase-1 levels in FLSs were assessed via immunofluorescence staining. Nuclei were stained with DAPI (blue) while NLRP3 and cleaved caspase-1 immunofluorescence is shown in green (scale bar = 50 μm). (**o**, **p**) The translocation of p65 (green) into nuclei (blue) was assessed (scale bar = 50 μm). (**q**, **r**) DCFH-DA was used to detect intracellular ROS levels (green) (scale bar = 50 μm). Data were presented as the mean ± SD from three independent experiments. $^{\#\#}P < 0.01$ vs. control; $^{*}P < 0.05$, $^{**}P < 0.01$ vs. TNF-α group.

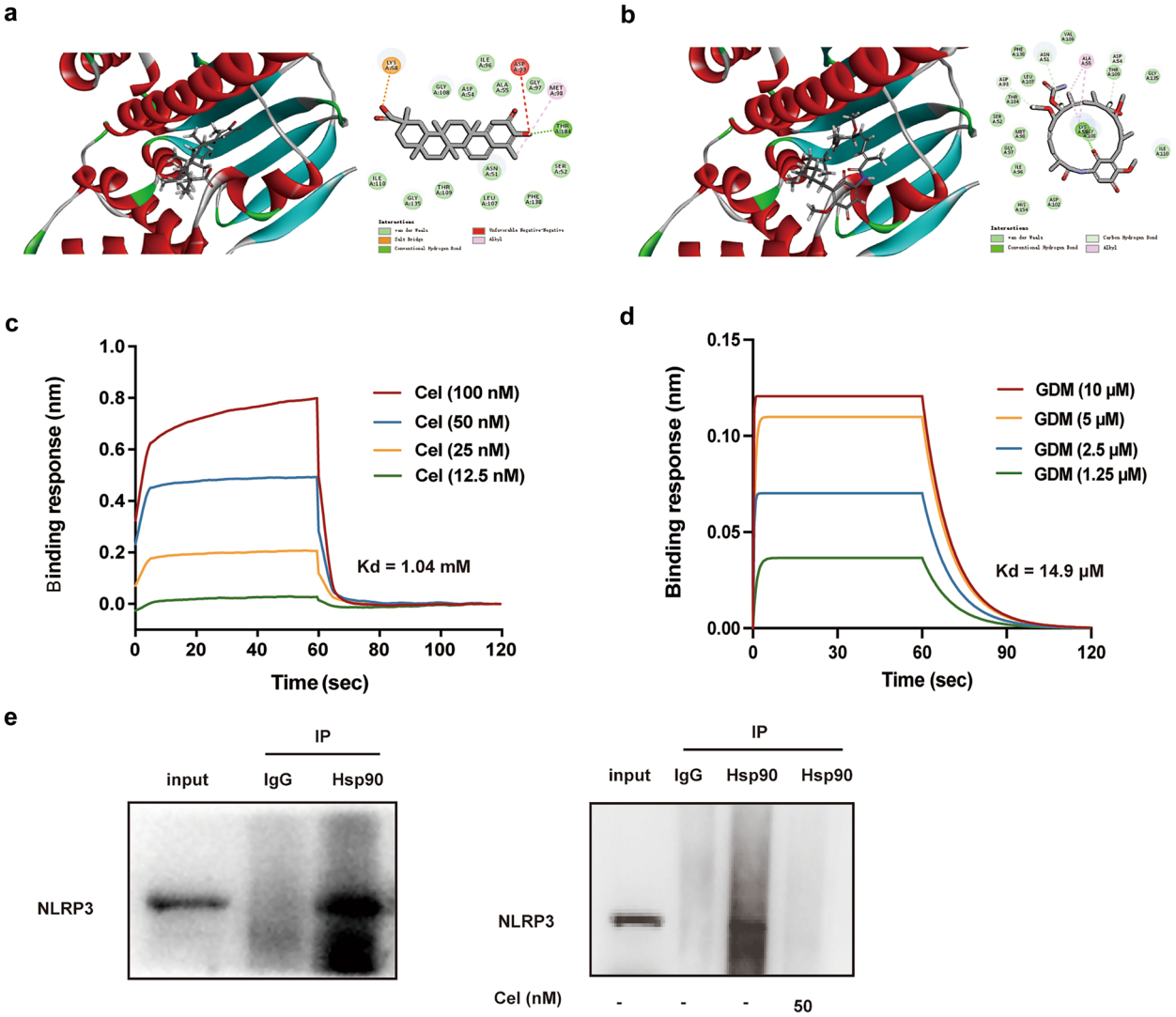

Fig. 6 Cel can inhibit the binding of Hsp90 to NLRP3 by binding to Hsp90. (**a**) The binding posture of Cel to Hsp90. (**b**) The binding posture of geldanamycin to Hsp90. (**c**, **d**) Binding response (nm) of Hsp90 to different concentrations of Cel and geldanamycin. Mixtures of different concentrations of Cel (12.5, 25, 50, and 100 nM) (**c**) or geldanamycin (1.25, 2.5, 5, and 10 μM) (**d**) with Hsp90 were measured using an Octet RED96 system. (**e**) Coimmunoprecipitation assay using FLSs treated with or without 50 nM Cel for 24 h. Cell lysates were immunoprecipitated with nonspecific IgG or an anti-Hsp90 antibody. FLSs that were not treated with Cel served as a positive control for IP with the anti-Hsp90 antibody. 'IgG' indicates the vehicle-treated cell lysates immunoprecipitated with nonspecific IgG. 'Input' indicates the whole cell lysates. Western blotting is representative of two independent experiments.

function of Cel is produced through the ROS-NF-κB-NLRP3 signaling pathway. However, is this the only way Cel inhibit the expression of NLRP3 inflammasome ?

There are literature reported that Cel is an Hsp90 inhibitor that can destroy the Hsp90-Cdc37 interaction in the superchaperone complex and induce the degradation of the Hsp90 client proteins Cdk4 and Akt to promote antitumor activity [34, 35]. Furthermore, Hsp90 is required for the activation of the NLRP3 inflammasome. NLRP3 is a client protein of Hsp90, and Hsp90 maintains the dynamic homeostasis of the protein by affecting the folding, activation, and stabilization of NLRP3 [36, 37]. Hsp90 regulates its client's function mainly through the following three mechanisms: promoting its steady-state

level and the level above the functional threshold, increasing its evolutionary ability, and triggering its stimulus-dependent activity [38, 39]. Moreover, studies have reported that NLRP3 is degraded by the proteasome if it does not bind to Hsp90 [21, 40].

However, whether Cel has a therapeutic effect on RA by inhibiting the regulation of NLRP3 by Hsp90 has not been confirmed. We studied the interaction between Cel and Hsp90 and the effect of Cel on Hsp90 and NLRP3 to further elucidate the mechanism by which Cel inhibits the NLRP3 inflammasome signaling pathway. Our molecular docking, Octet system, and co-IP assays revealed that Cel can directly interact with Hsp90. We also discovered that Cel inhibited the interaction between Hsp90 and NLRP3. This inhibition may be due to Cel inhibiting Hsp90 client signals and activity but not directly acting on the ATP-binding pocket of Hsp90 [41]. One of our most important results is to find that Cel plays a ' placeholder ' role by directly interacting with Hsp90, which in turn inhibits the binding of Hsp90 to NLRP3, thereby inhibiting its activation of NLRP3 inflammasome. This effect of Cel is not produced by directly binding to the active pocket of Hsp90, but by interfering with the distal binding signal of Hsp90. The above results indicate that Cel regulates the expression of NLRP3 inflammasome by inhibiting the upstream ROS-NF-κB signaling pathway and directly binding to Hsp90 to interfere with the activation of NLRP3.

However, whether Cel inhibits the formation of complexes between Cdc37 and Hsp90 through Hsp90, inhibits its ATPase activity and affects the stability of the Hsp90 client protein NLRP3, thus inhibiting the NLRP3 inflammasome in RA, remains to be further studied. Our subsequent experiments will involve the establishment of various cell models, the evaluation of the mechanism by which Cel affects RA from multiple perspectives, and further exploration of the regulatory relationship between Cel and Hsp90 and NLRP3.

CONCLUSION

In conclusion, Cel affects the activation and protein expression of NLRP3 inflammasome by inhibiting the upstream pathway and affecting the binding of NLRP3 inflammasome to its molecular chaperone, and exerting a protective effect on RA. Moreover, Cel not only relieves inflammation but also inhibits FLSs proliferation and migration and alleviates the symptoms of RA. This finding provides evidence for the antiarthritic properties of Cel and elucidates its potential molecular mechanisms in RA treatment.

SUPPLEMENTARY INFORMATION

The online version contains supplementary material available at https://doi.org/10.1007/s10753-024-02060-z.

ACKNOWLEDGEMENTS

The authors would like to thank the cells and technical support provided by Yantai University.

AUTHOR CONTRIBUTIONS

Junjie Yang conceived and designed the study. Junjie Yang and Biyao He performed the literature review and drafted the manuscript. Longjiao Dang and Jiayu Liu contributed to experimental data collection and analysis. Guohao Liu and Yuwei Zhao made investigation. Pengfei Yu and Qiaoyun Wang collected resources. Lei Wang and Wenyu Xin contributed to the critical revision of the manuscript. All authors approved the final manuscript and agreed to take responsibility for all aspects of the work.

FUNDING

This study was supported by the National Science Foundation of China (No. 81803546), the Natural Science Foundation of Shandong Province (No. ZR2018LH024) (No. ZR2017MH068) and the Shandong Laboratory Program (SYS202205).

DATA AVAILABILITY

All the data are contained within the manuscript and Supplementary Materials.

DECLARATIONS

Ethics Approval This study was conducted in accordance with the Declaration of Helsinki. The animal experiment was approved by the Animal Protection and Use Committee of Binzhou Medical University (2018-20).

Consent for Publication Not applicable.

Competing Interests The authors declare no conflict of interest.

REFERENCES

1. McInnes, I.B., and G. Schett. 2017. Pathogenetic insights from the treatment of rheumatoid arthritis. *Lancet* 389 (10086): 2328–2337.
2. Smolen, J.S., D. Aletaha, and I.B. McInnes. 2016. Rheumatoid arthritis. *Lancet* 388 (10055): 2023–2038.
3. Bartok, B., and G.S. Firestein. 2010. Fibroblast-like synoviocytes: Key effector cells in rheumatoid arthritis. *Immunological Reviews* 233: 233–255.
4. Friscic, J., M. Bottcher, C. Reinwald, H. Bruns, B. Wirth, S.J. Popp, K.I. Walker, J.A. Ackermann, X. Chen, J. Turner, et al. 2021. The complement system drives local inflammatory tissue priming by metabolic reprogramming of synovial fibroblasts. *Immunity* 54 (5): 1002.
5. Kumar, R.A., Y. Li, Q.J. Dang, and F. Yang. 2018. Monocytes in rheumatoid arthritis: Circulating precursors of macrophages and osteoclasts and their heterogeneity and plasticity role in RA pathogenesis. *International Immunopharmacology* 65: 348–359.
6. Sparks, J.A. 2019. Rheumatoid Arthritis. *Annals of Internal Medicine* 170 (1): Itc1–Itc15.
7. Cascao, R., J.E. Fonseca, and L.F. Moita. 2017. Celastrol: A spectrum of treatment opportunities in chronic diseases. *Frontiers in Medicine* 4: 69.
8. Xu, G., S. Fu, X. Zhan, Z. Wang, P. Zhang, W. Shi, N. Qin, Y. Chen, C. Wang, M. Niu, et al. 2021. Echinatin effectively protects against NLRP3 inflammasome-driven diseases by targeting HSP90. *JCI Insight* 6 (2): e134601.
9. Jing, M., J.J. Yang, L.R. Zhang, J. Liu, S. Xu, M.L. Wang, L.M. Zhang, Y. Sun, W.B. Yan, G.G. Hou, et al. 2021. Celastrol inhibits rheumatoid arthritis through the ROS-NF-kappa B-NLRP3 inflammasome axis. *International Immunopharmacology* 98: 107879.
10. Li, N., M.Y. Xu, B. Wang, Z.X. Shi, Z.H. Zhao, Y.Q. Tang, X.Y. Wang, J.B. Sun, and L. Chen. 2019. Discovery of novel celastrol derivatives as Hsp90-Cdc37 interaction disruptors with antitumor activity. *Journal of Medicinal Chemistry* 62 (23): 10798–10815.
11. Zhang, T., Y.Y. Li, Y.K. Yu, P. Zou, Y.Q. Jiang, and D.X. Sun. 2009. Characterization of celastrol to inhibit Hsp90 and Cdc37 interaction. *Journal of Biological Chemistry* 284 (51): 35381–35389.
12. Nizami, S., K. Arunasalam, J. Green, J. Cook, C.B. Lawrence, T. Zarganes-Tzitzikas, J.B. Davis, E. Di Daniel, and D. Brough. 2021. Inhibition of the NLRP3 inflammasome by HSP90 inhibitors. *Immunology* 162 (1): 84–91.
13. Luengo, T.M., M.P. Mayer, and S.G.D. Rudiger. 2019. The Hsp70-Hsp90 chaperone cascade in protein folding. *Trends in Cell Biology* 29 (2): 164–177.
14. Schopf, F.H., M.M. Biebl, and J. Buchner. 2017. The HSP90 chaperone machinery. *Nature Reviews Molecular Cell Biology* 18 (6): 345–360.
15. Sima, S., and K. Richter. 2018. Regulation of the Hsp90 system. *Biochimica Et Biophysica Acta-Molecular Cell Research* 1865 (6): 889–897.
16. Fouani, M., C.A. Basset, G.D. Mangano, L.G. Leone, N.B. Lawand, A. Leone, and R. Barone. 2022. Heat shock proteins alterations in rheumatoid arthritis. *International Journal of Molecular Sciences* 23 (5): 2806.
17. Rice, J.W., J.M. Veal, R.P. Fadden, A.F. Barabasz, J.M. Partridge, T.E. Barta, L.G. Dubois, K.H. Huang, S.R. Mabbett, M.A. Silinski, et al. 2008. Small molecule inhibitors of Hsp90 potently affect inflammatory disease pathways and exhibit activity in models of rheumatoid arthritis. *Arthritis and Rheumatism* 58 (12): 3765–3775.
18. Mayor, A., F. Martinon, T. De Smedt, V. Petrilli, and J. Tschopp. 2007. A crucial function of SGT1 and HSP90 in inflammasome activity links mammalian and plant innate immune responses. *Nature Immunology* 8 (5): 497–503.
19. Ruggiano, A., O. Foresti, and P. Carvalho. 2014. Quality control: ER-associated degradation: Protein quality control and beyond. *Journal of Cell Biology* 204 (6): 869–879.
20. Martinon, F., O. Gaide, V. Petrilli, A. Mayor, and J. Tschopp. 2007. NALP Inflammasomes: A central role in innate immunity. *Seminars in Immunopathology* 29 (3): 213–229.
21. Kelley, N., D. Jeltema, Y.H. Duan, and Y. He. 2019. The NLRP3 Inflammasome: An overview of mechanisms of activation and regulation. *International Journal of Molecular Sciences* 20 (13): 3328.
22. Haleagrahara, N., S. Miranda-Hernandez, M.A. Alim, L. Hayes, G. Bird, and N. Ketheesan. 2017. Therapeutic effect of quercetin in collagen-induced arthritis. *Biomedicine and Pharmacotherapy* 90: 38–46.
23. Brand, D.D., K.A. Latham, and E.F. Rosloniec. 2007. Collagen-induced arthritis. *Nature Protocols* 2 (5): 1269–1275.
24. Jia, Q., T.T. Wang, X.Y. Wang, H. Xu, Y. Liu, Y.J. Wang, Q. Shi, and Q.Q. Liang. 2019. Astragalin suppresses inflammatory responses and bone destruction in mice with collagen-induced arthritis and in human fibroblast-like synoviocytes. *Frontiers in Pharmacology* 10: 94.
25. Wang, M., H. Li, Y. Wang, Y. Hao, Y. Huang, X. Wang, Y. Lu, Y. Du, F. Fu, W. Xin, and L. Zhang. 2020. Anti-Rheumatic Properties of Gentiopicroside Are Associated With Suppression of ROS-NF-kappaB-NLRP3 Axis in Fibroblast-Like Synoviocytes and NF-kappaB Pathway in Adjuvant-Induced Arthritis. *Frontiers in Pharmacology* 11: 515.
26. Toh, M.L., S.S. Hong, F.V. Loo, L. Franqueville, L. Lindholm, W.V.D. Berg, P. Boulanger, and P. Miossec. 2005. Enhancement of adenovirus-mediated gene delivery to rheumatoid arthritis synoviocytes and synovium by fiber modifications: role of arginine-glycine-aspartic acid (RGD)- and non-RGD-binding integrins. *The Journal of Immunology* 175 (11): 7687–7698.
27. Li, Z., J.L. Guo, and L.Q. Bi. 2020. Role of the NLRP3 inflammasome in autoimmune diseases. *Biomedicine and Pharmacotherapy* 130: 110542.
28. Shen, H.H., Y.X. Yang, X. Meng, X.Y. Luo, X.M. Li, Z.W. Shuai, D.Q. Ye, and H.F. Pan. 2018. NLRP3: A promising therapeutic target for autoimmune diseases. *Autoimmunity Reviews* 17 (7): 694–702.
29. Sun, X.X., H.P. Pang, J.Q. Li, S.M. Luo, G. Huang, X. Li, Z.G. Xie, and Z.G. Zhou. 2020. The NLRP3 inflammasome and its role in T1DM. *Frontiers in Immunology* 11: 1595.
30. Corcoran, S.E., R. Halai, and M.A. Cooper. 2021. Pharmacological inhibition of the nod-like receptor family pyrin domain containing 3 inflammasome with MCC950. *Pharmacological Reviews* 73 (3): 968–1000.
31. He, Y., H. Hara, and G. Nunez. 2016. Mechanism and regulation of NLRP3 inflammasome activation. *Trends in Biochemical Sciences* 41 (12): 1012–1021.
32. Huang, Y., W. Xu, and R.B. Zhou. 2021. NLRP3 inflammasome activation and cell death. *Cellular & Molecular Immunology* 18 (9): 2114–2127.
33. Sharma, B.R., and T.D. Kanneganti. 2021. NLRP3 inflammasome in cancer and metabolic diseases. *Nature Immunology* 22 (5): 550–559.

34. Hoter, A., M.E. El-Sabban, and H.Y. Naim. 2018. The HSP90 family: structure, regulation, function, and implications in health and disease. *International Journal of Molecular Sciences* 19 (9): 2560.
35. Zhang, T., A. Hamza, X.H. Cao, B. Wang, S.W. Yu, C.G. Zhan, and D.X. Sun. 2008. A novel Hsp90 inhibitor to disrupt Hsp90/Cdc37 complex against pancreatic cancer cells. *Molecular Cancer Therapeutics* 7 (1): 162–170.
36. Chauhan, D., L. Vande Walle, and M. Lamkanfi. 2020. Therapeutic modulation of inflammasome pathways. *Immunological Reviews* 297 (1): 123–138.
37. Choudhury, A., D. Bullock, A. Lim, J. Argemi, P. Orning, E. Lien, R. Bataller, and P. Mandrekar. 2020. Inhibition of HSP90 and Activation of HSF1 Diminish Macrophage NLRP3 Inflammasome Activity in Alcohol-Associated Liver Injury. *Alcohol-Clinical and Experimental Research* 44 (6): 1300–1311.
38. Bohush, A., P. Bieganowski, and A. Filipek. 2019. Hsp90 and its Co-chaperones in neurodegenerative diseases. *International Journal of Molecular Sciences* 20 (20): 4976.
39. Kadota, Y., K. Shirasu, and R. Guerois. 2010. NLR sensors meet at the SGT1-HSP90 crossroad. *Trends in Biochemical Sciences* 35 (4): 199–207.
40. Sutterwala, F.S., S. Haasken, and S.L. Cassel. 2014. Mechanism of NLRP3 inflammasome activation. *Year in Immunology: Myeloid Cells and Inflammation* 1319: 82–95.
41. Hieronymus, H., J. Lamb, K.N. Ross, X.P. Peng, C. Clement, A. Rodina, M. Nieto, J.Y. Du, K. Stegmaier, S.M. Raj, et al. 2006. Gene expression signature-based chemical genomic prediction identifies a novel class of HSP90 pathway modulators. *Cancer Cell* 10 (4): 321–330.